Ground-Based Remote Sensing of Stratocumulus Properties during CLARA, 1996

R. BOERS,* H. RUSSCHENBERG, J. ERKELENS, AND V. VENEMA

International Research Center for Telecommunication–Transmission and Radar, Delft Technical University, Delft, Netherlands

A. VAN LAMMEREN

Royal Netherlands Meteorological Institute, De Bilt, Netherlands

A. APITULEY

Rijksinstituut voor Volksgezondheid en Milieuhygiene, Bilthoven, Netherlands

S. JONGEN

Eindhoven University of Technology, Eindhoven, Netherlands

(Manuscript received 20 July 1998, in final form 31 March 1999)

ABSTRACT

A method is presented to obtain droplet concentration for water clouds from ground-based remote sensing observations. It relies on observations of cloud thickness, liquid water path, and optical extinction near the cloud base. The method was tested for two case studies (19 April 1996 and 4 September 1996) during the Clouds And Radiation experiment (CLARA). The CLARA experiment was designed to observe clouds using a variety of remote sensing instruments near the city of Delft in the western part of the Netherlands. The measurement of cloud thickness is dependent on the detection of cloud base by lidar and cloud top by radar. It is shown that during CLARA it was possible to detect cloud base with an uncertainty of less than 30 m using current lidar techniques. The agreement between in situ and remote sensing observations of droplet concentration was reasonable. An error analysis indicates that this method is most sensitive to uncertainties in liquid water path and the unknown effects of multiple scattering on lidar signal returns. When the liquid water path is very small the relative error of the liquid water path increases to unacceptable levels, so that the retrieval of droplet concentration becomes very difficult. The estimated uncertainty in the strength of multiple scattering can explain differences between observations and retrievals of droplet concentration on one day, but not the other.

1. Introduction

With the advent of modern satellite systems it will be possible within the next 20 years to observe important climate parameters remotely with unsurpassed time and spatial resolution. The future function of these systems is, to a large extent, dependent on today's development of detection techniques of climate parameters from ground-based remote sensing. Similarly, where climate parameters are already measured from space, their value is inevitably linked to accurate validation at the ground.

The four most important parameters linking clouds to climate are cloud fraction, cloud optical depth, cloud droplet effective radius, and cloud droplet concentration. Optical depth is a measure of the reflective capacity of a cloud and, together with cloud fraction, is linked to cloud albedo. It is a function of the cloud liquid water path and the cloud droplet effective radius (Stephens 1978). Cloud droplet effective radius is inversely proportional to the one-third power of the droplet concentration (Twomey et al. 1984), which, in turn, is determined by local availability of anthropogenic and naturally occurring cloud condensation nuclei. So, variability in effective radius is determined by industrial activity and by continental–maritime transitions.

Han et al. (1994) used the International Satellite Cloud Climatology Project dataset to obtain global coverage of cloud optical depth and droplet effective radius.

* On leave from CSIRO Atmospheric Research, Aspendale, Australia.

Corresponding author address: R. Boers, CSIRO Atmospheric Research, Private Bag 1, Aspendale VIC 3195, Australia.
E-mail: reinout.boers@dar.csiro.au

They found broad confirmation of the expected differences between the Northern and Southern Hemispheres, as well as between land and ocean. However, their necessary reliance on satellite technology developed 20 yr ago implies that the technique to retrieve cloud droplet effective radius is uncertain; the satellite radiometer wavelength channel is broad and located in a portion of the wavelength spectrum where atmospheric emission is problematic. Validation procedures are essential to ascertain whether these techniques deserve their wide usage in remote sensing research.

Boers (1997) presented one such validation tool. In the context of obtaining long time series of cloud microphysical parameters for monitoring purposes at the Cape Grim Air Pollution Baseline Station at the northwest coast of Tasmania, he used a ground-based microwave radiometer, collocated with a pyranometer, to retrieve cloud droplet concentration and optical depth. He demonstrated that it is possible to distinguish between clouds of oceanic and continental origins. However, the technique is invalid at night, as it is dependent on solar irradiance; in addition, it cannot be used when multiple cloud layers, or ice clouds, are present. Boers' (1997) technique to retrieve cloud optical depth is very similar to techniques developed to retrieve optical depth from arctic stratus (Leontyeva and Stamnes 1994; Leontyeva et al. 1994) and Northern Hemisphere midlatitude stratus (Dong et al. 1997, 1998).

Frisch et al. (1995) utilize a combination of 35-GHz radar and microwave radiometer to retrieve the droplet number concentration of stratus clouds. In that study the radar was used to estimate the cloud thickness and vertical distribution of liquid water in the clouds. The method described in this paper utilizes lidar to estimate the cloud base, because it is a more reliable instrument than radar for that purpose, as will be shown below. Politovich et al. (1995) uses a microwave radiometer and cloud radar to estimate the liquid water content in mixed clouds; no attempt is made, however, to retrieve the droplet number concentration. In several studies (Fox and Illingworth 1997; Paluch et al. 1996; Sassen and Liao 1996) power-law relations between the radar reflectivity and the liquid water content are assessed for their use in retrievals. In the case of stratocumulus the radar reflectivity is determined by Rayleigh scattering, which limits the applicability of power-law relations to thin clouds in which no large drops are present (Papatsoris 1994). Doppler radars can be used to estimate the drop size distribution from the velocity spectrum (Gossard et al. 1997; Babb et al. 1999), but these methods rely on a careful interpretation of the effects of turbulence and differences in terminal fall velocity on the shape of the spectra.

In this paper a new technique is outlined to obtain droplet concentration from ground-based remote sensing. It requires the synergism of three collocated remote sensing devices, namely a cloud radar, a lidar, and a microwave radiometer. Using a limited dataset it is demonstrated that the technique yields results that are in broad agreement with in situ cloud observations.

The remainder of the paper is organized as follows. First, the theory will be presented whereby droplet concentration can be obtained from cloud thickness, liquid water path, and (partial) extinction profiles. Next, the different remote sensing instruments will be introduced as well as ways to derive the relevant cloud parameters. Then, the droplet retrieval method will be tested using selected observations during CLARA, and we present an error analysis to assess the validity of the method. We close with a set of conclusions.

2. Theory

The present technique is based on the inherent link between cloud optical extinction, cloud liquid water, and cloud droplet concentration. Boers and Mitchell (1994) discussed this link in detail. They followed well-established thermodynamic principles to describe the shape of extinction and liquid water content profiles with height above cloud base. They used the fact that cloud droplet distributions can be adequately described by gamma distributions. We do not repeat their analysis but merely state the result that the extinction σ can be formulated as

$$\sigma = \pi^{1/3} Q A(\alpha) \left(\frac{4}{3}\frac{\rho_w}{\rho_0}\right)^{2/3} A_d^{2/3} (1 - D)^{2/3} N^{1/3} (z - z_B)^{2/3}, \quad (1)$$

where Q is the extinction efficiency at visible wavelengths ($\approx$2), A_d is the vertical gradient of liquid water content under adiabatic conditions, N is the cloud droplet concentration, D is a parameter designating the departure from adiabatic conditions (Betts 1983), ρ_w is the density of liquid water, ρ_0 is the density of dry air, z is height, z_B is cloud-base height, and $A(\alpha)$ is defined as

$$A(\alpha) = \left[\frac{(\alpha + 2)(\alpha + 1)}{(\alpha + 3)^2}\right]^{1/3}, \quad (2)$$

where α is the exponent of the size parameter r in the gamma distribution that describes the droplet size distribution. Normally, an error of about 6%–8% is introduced by assuming a constant value for N (Boers and Mitchell 1994). However, the data to be shown later suggest that, on average, N was constant with height. In this model it is further assumed that α is constant with height. This is a good assumption as can be judged from calculations of this parameter from in situ droplet size distributions, although it may vary slightly from day to day. Although the assumption that $Q \approx 2$ is not valid for the smallest droplets (<1 μm), this will only affect a minor part of liquid water. We calculated that for a typical value of $N = 200$ cm^{-3} cloud droplets embedded in an adiabatic parcel just 5 m above cloud base would already have a mean radius exceeding 2 μm, those that are 10 m above cloud base would have a

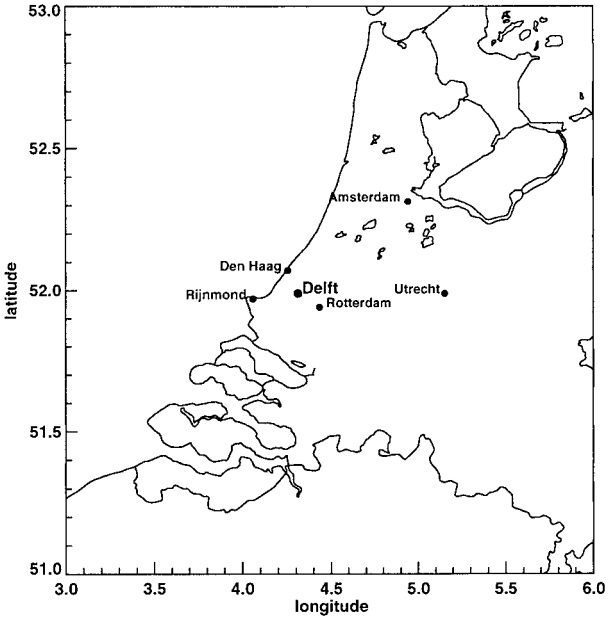

FIG. 1. Map of the western part of the Netherlands near the city of Delft. The location of the remote sensing equipment was at 51.99°N, 4.23°E.

mean radius of 4 μm. Therefore, even for shallow clouds the assumption that $Q \approx 2$ is not restrictive.

The value of A_d is a function of temperature and care has to be taken to make a proper choice for its use in individual applications. The best approach is to estimate cloud temperature from an infrared radiometer, which was available during CLARA as will be shown below. However, when cloud temperature is not available it can be estimated from radiosondes, or by extrapolation of the surface temperature to cloud base using the adiabatic assumption.

The liquid water content (LWC) varies linearly with height as

$$\mathrm{LWC} = A_d(1 - D)(z - z_B), \tag{3}$$

so that the liquid water path (LWP) is defined as

$$\mathrm{LWP} = \frac{1}{2}A_d(1 - D)h^2, \tag{4}$$

where h is cloud thickness.

The procedure we propose to retrieve droplet concentration can be summarized into five steps: 1) determine the cloud thickness h from a combination of lidar and radar data; 2) determine LWP from the microwave radiometer data; 3) use Eq. (4) to obtain D; 4) determine lidar extinction profiles with a profile inversion technique, for example the one developed by Klett (1983, see below); and 5) use D to regress in a least squares sense Eq. (1) to the extinction profiles with N as a free parameter.

Steps 1–3 yield values of the departure of the cloud from its adiabatic state. A value $D = 0$ implies that the layer is adiabatic; for D larger than 0 is implied the progressive departure of cloud liquid water from the adiabatic value. In step 5, increasing (decreasing) N increases (decreases) the model extinction near cloud base, providing the method to minimize the sum of squares of the difference between the extinction retrieval profiles and the extinction model. The value of N at this minimum is the final retrieval product.

3. Measurements

a. Introduction

CLARA took place in 1996 near Delft, in the heavily populated industrial heart of Netherlands. The instruments were located on the top of a 21-floor building at an altitude of 95 m on the campus of Delft Technical University (51.99°N, 4.02°E) 1 km south of the city center. The location is 10 km southeast of Den Haag, and 8 km northwest of Rotterdam; the Rijnmond industrial area is 20 km to the southwest (Fig. 1). The study focuses entirely on stratocumulus water clouds. Table 1 summarizes the different instruments, which are described below in more detail.

b. Radar

The Delft Atmospheric Research Radar (DARR) is a dual antenna FM–CW radar (3.315 GHz), with a range resolution of 15 m. It has been in operation since 1983 and has primarily been used in studies of stratified precipitation systems (Russchenberg 1992). For this frequency, the scattering from clouds is in the Rayleigh regime, so that large precipitating particles (100–200 μm) contribute several orders of magnitude more to the scattering return than do suspended cloud droplets (10–30 μm). As a result the detection of cloud base, where suspended cloud droplets are small and precipitation

TABLE 1. Summary of ground-based remote sensing instruments during CLARA (n.a. = not applicable).

Instrument	Frequency or wavelength	Range resolution (m)	Temporal resolution (s)	Product used in this study
Radar	3 GHz/10 cm	15	5.12	cloud top
Lidar CT75	1 μm	30	30	cloud base and extinction
Lidar HTRL	1 μm	5	0.1	cloud base and extinction
IR radiometer	9.6–11.5 μm	n.a.	1	cloud-base temperature
Microwave radiometer	20/30/50 GHz	n.a.	1	liquid water path, water vapor path

droplets are large, is often not possible. Near cloud top, the suspended cloud droplets are the largest, and precipitation particles are frequently absent. Therefore, detection of cloud top is more straightforward. As the wavelength of DARR is considerably longer than that of the more frequently used 94-GHz cloud radars, temperature and humidity fluctuations can contribute to the backscatter returns when stratocumulus or cumulus clouds are probed. Fortunately, most temperature and humidity fluctuations occur exactly near cloud top because cloud-top infrared cooling is the primary agent responsible for the onset of turbulence underneath the overlaying temperature and humidity discontinuity.

The procedure for extracting cloud height from radar returns is to locate the maximum power of the range-corrected radar returns, searching from the top downward. Once the maximum has been located, the height of the 10% level of the maximum (above the maximum) is designated as cloud top. The 10% level was chosen after careful inspection of the data and assures that single data points exceeding the noise floor are not designated as cloud top. This technique has been tested for several case studies during CLARA with good results (Russchenberg et al. 1998).

It might be argued that direct *Z*–LWC relations should be used to infer cloud properties. However, *Z*–LWC relations suffer from the influence of large drops on the reflectivity factor, thereby limiting the accuracy. Furthermore, at 3 GHz, radars are susceptible to Bragg scatter due to refractive index fluctuations and particulate scatter by cloud droplets (Gossard and Strauch 1983; Knight and Miller 1998). The radar is thus only used to estimate the cloud top. So, in principle, it could be replaced by other observation tools that can measure the cloud top (for instance, a lidar or a radar from a space platform).

c. Lidar

Two lidars were operated during the campaign. The first was a Vaisala cloud-base lidar (CT75K), operated by the Royal Netherlands Meteorological Institute (KNMI). It is an eye-safe diode laser (InGaAs) operating at 0.905 μm with a pulse repetition rate of 5.13×10^3 Hz yielding an average return every 30 s. It is a fully automated system for which individual normalized, range-square corrected, shot profiles at a range resolution of 30 m are stored. The second lidar is a flash lamp–pumped Nd:Yag lidar operating at 1.06 μm with a frequency of 10 Hz and a range resolution of 15 m. This instrument, the High Temporal Resolution Lidar (HTRL), is not eye safe and is operated by the National Institute of Public Health and the Environment (RIVM). The range-gating accuracy of the radar and CT75 lidar was cross-checked by measuring the distance of a building 1200 m from the experiment site. Both instruments agreed upon the distance to within a few meters.

While the CT75K is suited for long-term monitoring of cloud base, the HTRL is ideal for high-resolution sampling of the boundary layer underneath the cloud. The CT75K will be used to invert the lidar profiles, while the HTRL will be used to provide the high-resolution imagery.

A comparative study was carried out to assess the differences in backscatter returns from the CT75K and the HTRL (Apituley et al. 1998). Both systems were synchronized and 30-s-averaged shot profiles were compared. For low- and midlevel clouds the backscatter profiles agreed very well, but for high-level clouds some differences occurred that require further investigation.

The short wavelengths associated with the lidars imply operation in the Mie-scattering regime. Stable inversion techniques are available to convert the raw attenuated backscatter profiles into extinction profiles (Klett 1983; Fernald 1984), and rely on the assumption that the backscatter and extinction are proportional to each other. This assumption is excellent for water clouds, as any Mie calculation will attest. It then becomes possible to cast the lidar signal return equation into a homogeneous Ricatti equation, which has an analytic solution for the extinction factor.

The procedure to detect cloud base commences with a profile inversion (Klett 1983), yielding partial extinction profiles. Cloud base is identified as the height level on the digitized extinction curve (30-m resolution) immediately below the level at which the signal extinction exceeds the value of 2 km^{-1}, yielding a first estimate of cloud base and a portion of the extinction profiles directly above cloud base. A typical height at which the lidar signal is extinct is 90 to 150 m above cloud base. The range resolution of 30 m implies that 3–5 extinction data points per profile can be used to regress against Eq. (1).

Further refinements to the procedure to detect cloud base are implemented when the functional form of the extinction as represented by Eq. (1) is fitted through the measured extinction profile. Then, the optimum solution that reduces the rms error between the theoretical and measured extinction curve is calculated. The refinement to detect cloud base involves a two-step process. In the first step, given the value of D and a set of points on the extinction profile, we use two free parameters z_B and N in the regression rather than only one (N). The two restrictions are that there are at least three points on the extinction curve, and, of course, that z_B lies between the initial estimate of cloud base and the next range point on the lidar signal profile. After this first regression the new cloud base value is now located between two points on the original extinction profiles separated by 30 m. The new value for z_B is used to update D using Eq. (4) while leaving LWP constant. Using the new value of D, which is typically between 0.01 and 0.07 different from the original value, a final regression of the theoretical extinction curve to the observations is performed as a second step. Excellent fits can be obtained between a lidar-retrieved extinction curve (triangles) and a mod-

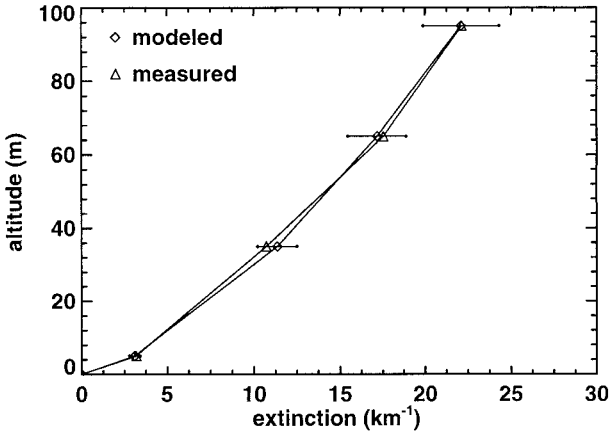

FIG. 2. Measured (triangles) and modeled (diamonds) extinction profiles.

eled extinction curve (diamonds; Fig. 2). The error bars indicate the shape change in the theoretical extinction curve for a 30% change in droplet concentration from its optimum value.

The most serious problem associated with this technique is the imprecision of the calculated extinction profiles due to the unknown contribution of multiple scattering. There are many studies in the literature proposing treatments for this problem (Young 1995), but none give a completely satisfactory solution. Multiple scattering is a function of the field of view of the lidar, the distance of the lidar to the cloud, the phase function of the particles, the concentration of droplets, and the optical depth of the cloud. For some applications multiple scattering can seriously affect the inversion of lidar profiles, such as when the cloud is very distant from the receiver (Spinhirne et al. 1989). De Wolf et al. (1999), who proposed a model of multiple scattering applicable to the lidar in the CLARA setup, found that multiple scattering for this type of systems with the cloud near to the receiver is negligible for optical depths less than 20. So, in our study it will be neglected in the regression to obtain the droplet concentration. However, we will take it into account when considering the uncertainty of the retrieval (see below). At any rate, it should be recognized that individual lidar systems would need to be evaluated on potential multiple scattering problems when retrievals of the kind described in this paper are attempted.

d. Microwave radiometer

The microwave radiometer used during the experiment is a Rescom noise injection radiometer operating at 21.3, 23.6, and 31.7 GHz. The first two frequencies are near the water vapor absorption peak of 22.3 GHz. The third frequency is more sensitive to liquid water absorption. This system is operated by Eindhoven Technical University and represents mature technology for which many retrieval algorithms for water vapor path and liquid water path are available. The retrieval algorithm applied in this paper uses the 21.3- and 31.7-GHz channels and is an adaptation of the Peter and Kämpfer (1992) algorithm. The algorithm of Peter and Kämpfer (1992) has been modified to improve the retrievals of liquid water path. Radiosonde measurements are used to obtain the temperature and pressure profiles and the initial water vapor profile. The initial profiles are multiplied each with a tuning parameter to match the measured brightness temperatures. Details of the algorithm can be found in Erkelens et al. (1998a,b). The use of radiosondes and radar data can improve the retrieval of liquid water path, because it fixes the cloud temperature. Errors in the estimated cloud temperature can strongly influence the retrievals (see, e.g., Westwater and Guiraud 1980).

e. In situ cloud probe

On selected days it was possible to fly an instrumented aircraft near the central site of the experiment. The aircraft (PA 31 Navajo Chieftain two-engine turboprop) was fitted with a forward-scattering spectrometer probe (PMS-FSSP-100) sensitive to particles with diameters between 1 and 47 μm. The probe also detects the number of particles exceeding the upper-range limit, but cannot provide estimates of the size of those particles. The 15 size bins of the FSSP were used to derive liquid water content, effective radius, mean radius, and droplet concentration at a 1-s time resolution.

Values for $A(\alpha)$ [Eq. (2)] can be evaluated from α, which in turn can be calculated in a straightforward manner from the fraction of the mean and effective radius $r_{\text{mean}}/r_{\text{eff}} = (\alpha + 1)/(\alpha + 3)$ using the properties of the gamma distribution used to represent the droplet spectra. The value of α varied somewhat with height but on average it was around five on 19 April and around seven on 4 September. So, under the range of observed clouds, A varies tightly between 0.869 and 0.896. In the subsequent analysis we use the above values for α. However, we return to the problem of assigning a proper value for α in the analysis of uncertainties.

Severe flight restrictions caused by heavy traffic in the vicinity of the Schiphol (Amsterdam) and Zestienhoven (Rotterdam) Airports precluded frequent passes directly overhead of the ground-based equipment. On both days the data were taken to the west and southwest of Delft in flights of 2-h duration with only a few direct overpasses. Clearly, there is some averaging of cloud inhomogeneities involved by including all such flight data.

f. Radiosondes

Vaisala radiosondes were launched at 4-h intervals, providing temperature, relative humidity, wind speed, and wind direction as a function of altitude. The top of

the boundary layer was determined from the jumps in temperature and humidity across the interface with the overlying air. These measurements were used to verify the exact location of the atmospheric boundary layer top. Individual profiles of temperature or water vapor cannot necessarily be used to obtain accurate information about the cloud liquid water adiabatic structure. The reasons are that, on ascent into cloud, probe wetting may reduce the recording temperature and that, as a rule, there are hysteresis effects influencing the measurements.

g. Infrared radiometer

The value of the cloud-base temperature is important since it fixes the value of the vertical gradient of the adiabatic liquid water content A_d. A narrow field of view (50-mrad field of view) infrared radiometer, sensitive in the 9.6–11.5-μm range, was used to detect cloud-base temperature between $+50°$ and $-50°$C with an accuracy of 1.5°C. To obtain this accuracy the temperature of the radiometer housing is stabilized at 35°C, while a precipitation detector controls the cover to shield the sensor in case of rain. On 4 September, cloud-base temperature was about 8°C, while on 19 April it was only 2°C. For this range of temperatures the change in A_d is 15%, varying from 0.15×10^{-5} kg kg^{-1} m^{-1} at 2°C to 0.17×10^{-5} kg kg^{-1} m^{-1} at 8°C.

4. Results

a. The interpretation of lidar and radar signals

The interpretation of lidar and radar signals is not a trivial matter. The identification of cloud base or cloud top in signal returns depends on a careful examination of individual profiles. Signal scatterers other than cloud droplets may, in part, obscure the cloud boundary. Examples for such problems in the interpretation of lidar signals are the presence of drizzle droplets or aerosol near cloud base, which can potentially ''smooth out'' the signals. Examples for radar returns are drizzle droplets, the presence of a few of which can far dominate the signals from cloud droplets, and Bragg-type scattering. In fact, without the use of a Doppler capability to detect drizzle, it is almost impossible to detect cloud base with radar.

Bragg-type scattering is coherent scattering coming from small-scale fluctuations in the refractive index (Knight and Miller 1993). Knight and Miller (1998) have attempted to separate the Bragg from cloud particulate scattering and identified regions at the outer edges of clouds (''mantle echoes''), where Bragg scattering can be large because of large gradients in moisture. Although a thorough investigation of the relative importance of scatterers contributing to a radar or lidar signal is beyond the scope of this study, it is nevertheless important to ascertain whether the lidar and radar can detect the clouds. For this reason we modeled the cloud returns for both the radar and the lidar using the FSSP droplet spectral data taken during the 19 April 1996 flight.

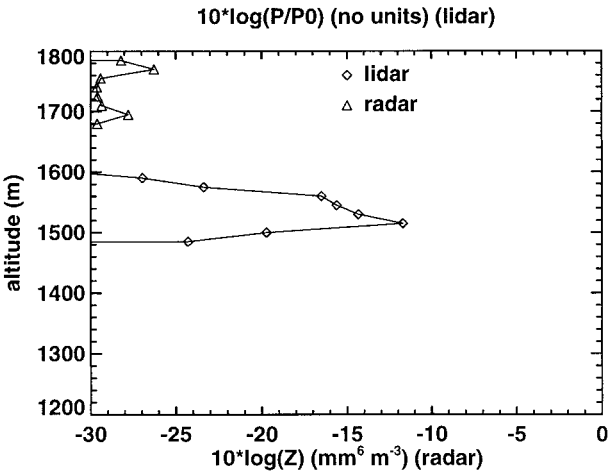

FIG. 3. Radar (triangles) and lidar (diamonds) data (19 Apr 1996, near 0630 UTC). Radar data are represented in dBZ [10 log(Z) (mm^6 m^{-3})], which is the unit most commonly used in radar research. Lidar data are dimensionless.

Figure 3 shows the radar reflectivity (triangles) in dBZ (10 log of radar reflectivity in units of mm^6 m^{-3}, the usual radar unit) where the signal has been simulated from droplet spectra taken on 19 April 1996 (around 0630 UTC). The noise floor of DARR is at -30 dBZ, which implies that the radar signals due to suspended cloud droplets between 1680 and 1780 m are above the noise floor, regardless of the presence of Bragg scattering or drizzle droplets.

For comparison with the radar data we also plotted the logarithm of the attenuated lidar backscatter profile $10 \log[P(z)/P(0) = \beta \exp(-2 \int \sigma\, dz')]$ (this quantity has no units), where β is the backscatter coefficient, similarly modeled from the droplet spectra measured at 0630 UTC 19 April 1996. The lidar signal does not penetrate the cloud beyond 1600-m altitude, only about 120 m above cloud base. The implication from Fig. 3 is that, regardless of the presence of alternative interpretations of the signals, the radar is able to detect cloud top but may not detect cloud base, while the lidar is able to detect cloud base but will not detect cloud top. So, in the application shown in this study both instruments are essential for the detection of cloud thickness.

b. Case studies

The observations to be shown were taken on 4 September 1996 (CLARA-II) and a short segment on 19 April 1996 (CLARA-I).

1) 4 SEPTEMBER 1996

On this day a weak cold front was stationary over the Netherlands north of Delft. The line of the front was

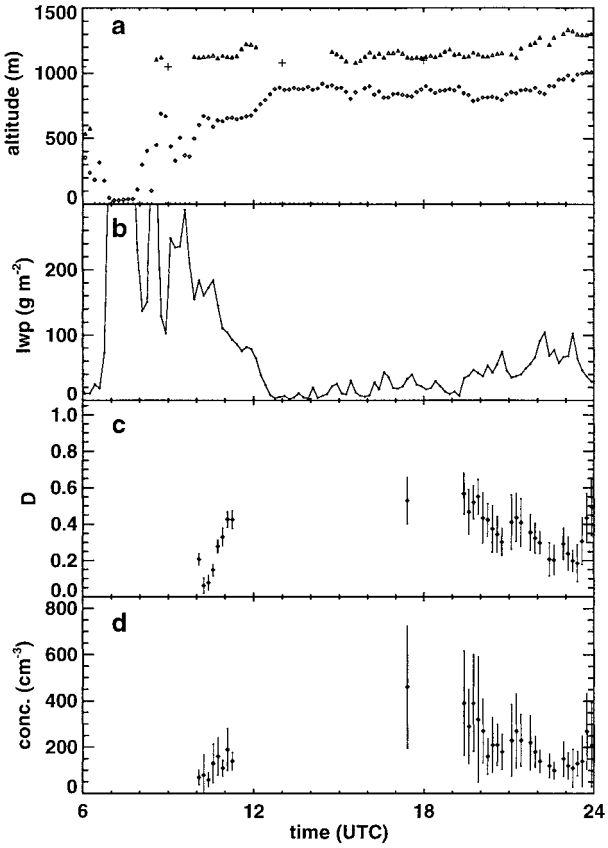

FIG. 4. (a) Time series of cloud base determined by lidar, and cloud top determined by radar for 4 Sep 1996. Individual points are 10-min averages. (b) Time series of microwave radiometer liquid water path on 4 Sep 1996. (c) Retrieval of parameter *D* for 4 Sep 1996. (d) Retrieval of droplet concentration for 4 Sep 1996.

roughly from west–south–west to east–north–east. Satellite imagery indicated that clouds had broken up entirely 50–100 km south of the front. However, just south of the front a thick band of clouds persisted in the morning hours (0400–0600 UTC) while Delft was engulfed in fog. Winds were from the northwest for the entire time for which observations were recorded (0400–0000 UTC next day), with little or no perceptible shift in wind direction at the time of frontal passage over Delft (just before 1200 UTC).

Figure 4a shows cloud base and cloud top as derived from the lidar/radar combination. As the front approached light drizzle fell between 0700 and 0800 UTC after which cloud base lifted rapidly from the surface to about 600 m. The cloud-base algorithm is able to separate drizzle returns from cloud-base returns because the signal strength of clouds far exceeds that of drizzle. From the time of frontal passage onward there was a period of 4 h during which cloud cover was not completely 100%. From about 1600 UTC onward cloud cover was almost 100% and cloud base slowly lifted to 950 m after 2000 UTC. The radar cloud tops coincide quite well with a temperature inversion as determined from radiosondes. These points are indicated as plus symbols on Fig. 4a. There are several times when it was impossible to determine cloud top, in particular near the frontal passage. After 1600 UTC cloud top lifted as well, so that the average cloud thickness remained constant.

Figure 4b shows the variation of liquid water path with time. Near 0800 UTC there is a discontinuity in water vapor (not shown) associated with a sharp peak in liquid water followed by a characteristic exponential decay. Both are associated with remnants of precipitation droplets evaporating on the aluminum reflector of the radiometer. Soon after the passage of the precipitation, the water vapor path values rose from 1.6 to over 2 cm, when a band of thick clouds passes the site (0800 UTC). Just before 1200 UTC there is a near discontinuous drop of 0.6 cm in water vapor path associated with the frontal passage. Cloud liquid water path was very small between 1200 and 1500 UTC after which it increased slightly as cloud cover thickened. Figures 4c and 4d will be described below, but are included here with the other two time series to facilitate comparison.

Between 0800 and 1100 UTC cloud-base height shows great variations. Some of these variations were caused by the presence of precipitation, which lowered cloud base. However, some variations are also associated with the presence of multiple cloud layers, and are especially evident just before 1000 UTC. A high-resolution picture of the attenuated backscatter profiles of the HTRL is shown in Fig. 5. At both sides of the 1000 UTC marker there are multiple cloud layers visible. Retrievals will not be performed when multiple cloud layers are present. Also, just before 0955 UTC and 1005 UTC, there are regions of enhanced backscatter below the cloud base (light gray area) associated with evaporating drizzle droplets falling below cloud base.

Aircraft observations originated from the airport of Zestienhoven (near Rotterdam) located 7 km to the southeast of Delft and were carried out between 0600 and 0900 UTC; several flight passes were carried out in the close vicinity to the west and south of Delft. Figure 6 (top) shows the droplet concentration as a function of height for aircraft latitudes south of 52.1°N. The measurements were scattered over two cloud layers, one between levels of 400 and 600 m, the other between 800 and 1000 m. As discussed above, when the presence of this (semitransparent) lower cloud layer was detected in the lidar signals, the remote sensing data were not included in the droplet retrievals. There were large variations in droplet concentration, but the 10-hPa averages fall within a tight range of 180–250 cm^{-3}. Clearly, the distribution of concentration values is asymmetric, with the arithmetic mean slightly elevated above the median values. Figure 6 (bottom) shows the liquid water content for the same time series; also shown is the adiabatic liquid water content as the thin straight line. The slope of this line is more critical than its intercept because it is difficult to ascertain the exact value of cloud base. This explains in part the presence of ''superadiabatic''

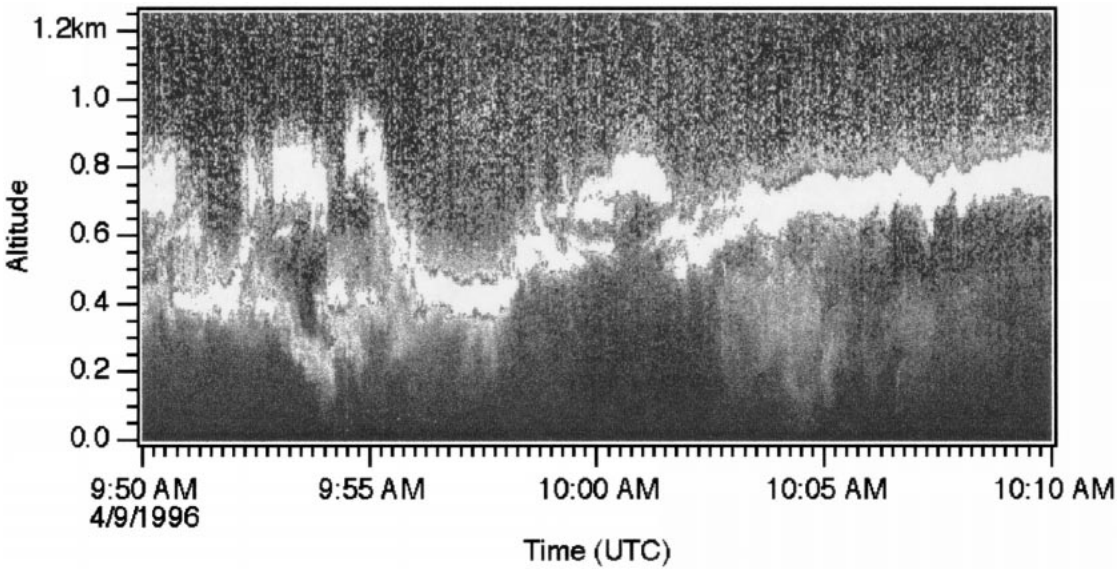

FIG. 5. Single shot resolution image of the range square corrected and normalized RIVM lidar attenuated backscatter data near 1000 UTC 4 Sep 1996.

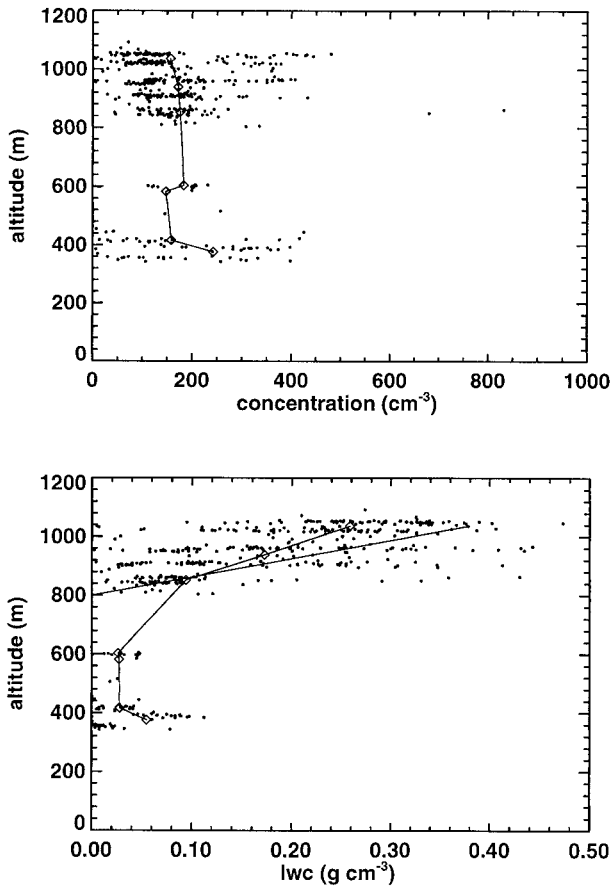

FIG. 6. (top) 100-m averaged droplet concentrations taken south of 52.1°N. Small dots are 10-s averages on 4 Sep 1996. (bottom) 100-m averaged liquid water contents taken south of 52.1°N. Small dots are 10-s averages on 4 Sep 1996. Thin straight line is the adiabatic liquid water content.

cloud liquid water points in the plot. The actually measured liquid water content increased much less rapidly than its maximum potential value as shown by the adiabatic liquid water content. The implication is that the layer is not well mixed.

Fig. 4c shows the time series of the 10-min-averaged retrieved parameter *D*. After the initial small values near 1000 UTC it increased rapidly to about 0.5 after 1100 UTC. As discussed above, just before 1000 UTC there were multiple cloud layers, and (evaporating) precipitation existing below cloud base. So, under these conditions, the idealized assumption used to perform the retrieval, namely a single nonprecipitating cloud deck, is not valid. Therefore, before the frontal passage the only valid results were obtained after 1000 UTC. Near noon, the liquid water path decreased rapidly as clouds broke up temporarily. Therefore, the relative uncertainty in LWP is unacceptably large and no *D* or *N* retrievals are possible until well after 1900 UTC, except for one occasional retrieval near 1730 UTC. The computations imply that during most of the day the cloud contained only roughly 50% of its possible adiabatic amount of liquid water. Interestingly, these results are not consistent with those of Albrecht et al. (1990) who reported mostly adiabatic clouds using a method very similar to ours. The reason for the difference is unclear. Adiabatic clouds can only exist if the boundary layer is perfectly well mixed and if entrainment is dominated by interfacial mixing. In case entrainment occurs on larger scales, or if the turbulence generated by processes in the cloud is weak, then well-mixed conditions are more difficult to maintain giving rise to subadiabatic liquid water profiles. For our case studies it is impossible to be more precise about the boundary layer turbulence

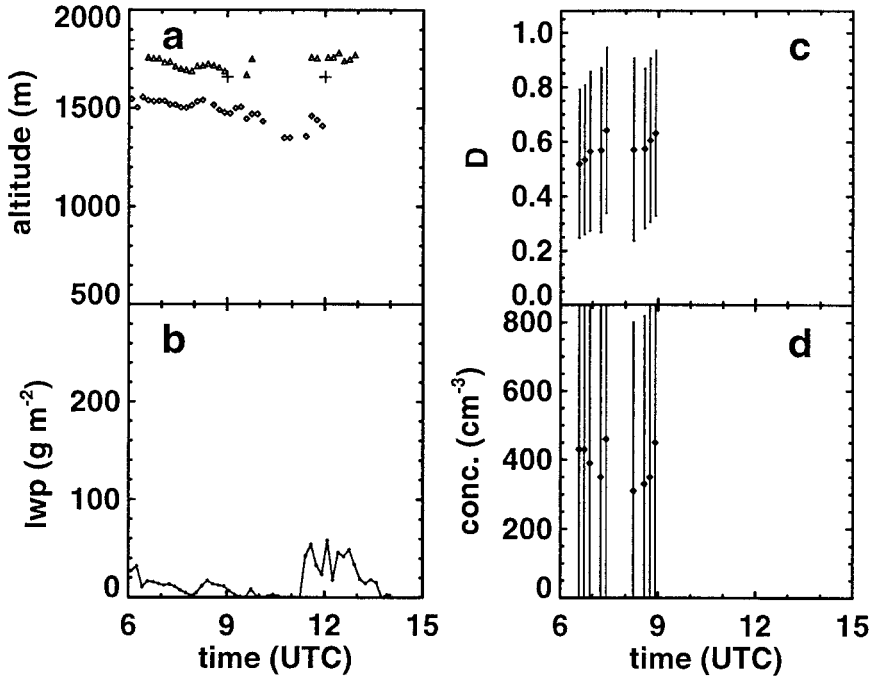

FIG. 7. (a) Time series of cloud base determined by lidar, and cloud top determined by radar for 19 Apr 1996. Individual points are 10-min averages. (b) Time series of microwave radiometer liquid water path on 19 Apr 1996. (c) Retrieval of parameter *D* for 19 Apr 1996. (d) Retrieval of droplet concentration for 19 Apr 1996.

structure as no turbulence probes were flown on the aircraft.

Figure 4d shows the 10-min averaged retrieval of the droplet concentration. This graph shows some similarity to Fig. 4c, due to the dependence of *N* on the parameter *D*. By and large, concentrations are restricted to values below 400 cm^{-3}. The first values on the plot after 1000 UTC were obtained very close to the time of overflights. The droplet retrievals range from 100 to 200 cm^{-3} underestimating the mean of the aircraft data by about 50%. After 1800 UTC, the LWP values increased again. Similarly, the mean of the retrievals of *N* increases to 100–400 cm^{-3}.

2) 19 APRIL 1996

On this day an anticyclone was located over eastern Europe with a low-pressure center between England and Iceland, directing a weak and mild southwesterly flow over the continent. An extended region of midlevel (3–5-km altitude) clouds persisted during the night and early morning giving way to a thin layer of stratocumulus clouds by 0600 UTC. This stratocumulus layer broke up before noon after which broken stratocumulus appeared. We focus our attention on the solid stratocumulus clouds in the early morning. Figure 7a indicates that this layer was located near 1600 m with a thickness of less then 250 m. The radiosonde observation at noon (a plus symbol) is 100 m lower than the corresponding radar top. On investigation of the radar profiles, this difference appears to be due to the inability of the radar cloud-top retrieval to detect cloud top because of the proximity of another overlying layer with a high, but unexplained, reflectivity. Consequently, the radar cloud tops between 1130 UTC and 1300 UTC are not accurate enough to perform retrievals. It indicates that great care has to be taken in interpreting such remote sensing information. The liquid water paths (Fig. 7b) are markedly smaller than on those observed on 4 September because clouds are thinner. Flight legs were flown within a distance of 50 km from the radar site to the southwest of Delft. The observed droplet concentrations have a very large spread ranging from 0 to 900 cm^{-3} (Fig. 8—top) while the liquid water contents vary between 0 and 0.39 g cm^{-3}. The 50-m average of the droplet concentration is constant at approximately 500 cm^{-3} except near cloud base. However, this may be fortuitous, as cloud base appeared to descend with time during the 2 h of flight, so that a mean ''cloud base'' is difficult to determine. There is a large cluster of data points at 1600 m of around 800 cm^{-3}, 0.25 g m^{-3} that appears to be removed from the rest of the points. This cluster was taken inside the cloud in the later part of the flight period, when the cloud was distinctly lower than it was earlier. We speculate that, given the southwesterly wind direction, the air parcels had probably traversed the industrial center of the Rijnmond area, resulting in enhancements to the droplet concentration.

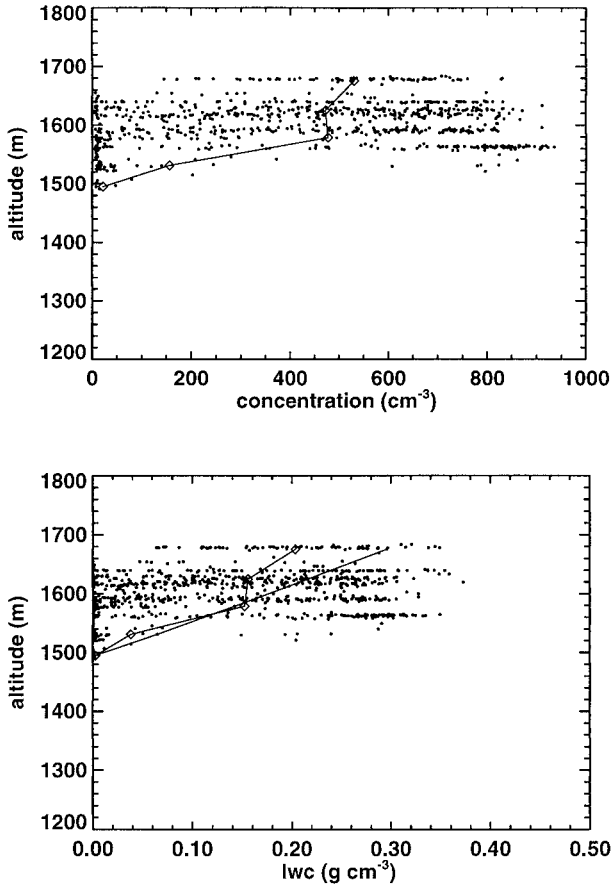

FIG. 8. (top) 50-m-averaged droplet concentrations taken south of 52.1°N. Small dots are 10-s averages on 19 Apr 1996. (bottom) 50-m-averaged liquid water contents taken south of 52.1°N. Small dots are 10-s averages on 19 Apr 1996. Thin straight line is the adiabatic liquid water content.

Figure 7c indicates once again that D is around 0.6. Although only a few valid retrievals were obtained before 0900 UTC, they reasonably well follow the in situ data taken directly overhead (400–600 cm^{-3}, Fig. 7d). However, as was the case for the previous case study, they underestimate the mean of the observations, in this case by 20%.

3) UNCERTAINTIES AND LIMITATIONS

The vertical bars plotted on Figs. 4 and 7 indicate the uncertainty determined by a procedure explained in the appendix. Uncertainties are larger on 19 April than on 4 September. The uncertainty in D is generally less than 0.1 on 4 September before frontal passage and increases to 0.15 after 1900 UTC; it exceeds 0.2 on 19 April. The uncertainty in N is less than 100 cm^{-3} before noon on 4 September and varies between 50 and 200 cm^{-3} after 1900 UTC. On 19 April it is very large and exceeds 400 cm^{-3}.

We compute the mean values for the droplet retrievals for the time period before noon on 4 September, and that of the entire period on 19 April, and compare them with the observed concentrations for the same day. The values of the retrieved/observed concentrations in cm^{-3} are: 117 ($\pm$65)/170 (4 September) and 395 ($\pm$430)/500 (19 April). The retrievals of 19 April may seem to be unacceptable because of their large uncertainty. However, we chose to include this day in the analysis because the retrievals appear to be consistent with each other, and because the value of the uncertainty divided by the square root of the number of observations is considerably less, namely 178 cm^{-3}. For both the retrievals and observations, the droplet concentrations are a factor of three higher on 19 April than on 4 September, although the retrieval underestimates the mean of the observations by 45% on 4 September, and by 20% on 19 April.

One possible reason for such an underestimate is the effect of the unknown multiple scattering. If multiple scattering cannot be neglected, then the apparent extinction would be, in reality, larger than that retrieved by our method. This implies that the retrieved droplet concentration is underestimated, which can be estimated by repeating the calculations using a different value for η, the multiple scattering factor (see appendix). In the original calculation $\eta = 1.0$, that is, no multiple scattering. In the sensitivity analysis we chose a value of $\eta = 0.9$. For this value the apparent extinction in the cloud would increase by 8%–10%. Recalling that the error bars on the extinction curve in Fig. 3 imply a 30% change in droplet concentration, then the droplet concentration would increase by a little less than 30% in case we underestimate the effect of multiple scattering. This is insufficient to account for the difference between the observations and the retrievals on 4 September, but could account for the differences on 19 April.

An error in the retrieval can occur because of errors in α, which are normally not known a priori. The reason is that in situ data are usually not available when remote retrievals of droplet concentration are performed. As an example, on 19 April a 3% error in the modeled extinction may be incurred by using the relatively imprecise value of $\alpha = 7$ in the model rather than the average observed value of $\alpha = 5$ on this day. Under those conditions the value of $A = 0.896$ is 3% higher than the value that it should have been, namely $A = 0.869$. The model would attempt to compensate for this by retrieving a lower value for N by about 8%.

Finally, a limitation to the retrieval technique is that retrievals cannot be performed when significant drizzle is present. Under these conditions the droplet spectra would be bimodal and an unknown amount of liquid water path would be present in the second, drizzle mode for which our extinction model is invalid. These conditions ceased to exist just after 1000 UTC on 4 September, which is the starting point for all retrievals, and were not present on 19 April.

5. Conclusions

We have shown that it is possible to retrieve droplet concentration from a combination of microwave radiometer-, lidar-, and radar-derived cloud parameters. The cloud parameters include cloud base and (partial) cloud-base extinction profiles (lidar), cloud top (radar), and liquid water path (microwave radiometer). The retrieval algorithm uses the assumption that the droplet concentration is constant with height inside the cloud, and that there are no multiple cloud layers. The algorithm was tested for two case studies taken during CLARA when stratocumulus clouds prevailed at the remote sensing site. The assumption of a constant droplet concentration was good for the two case studies.

On both days the retrievals underestimate the in situ aircraft observations, on 4 September by 45%, and on 19 April by 20%, but the factor-of-three difference in concentration between the two case studies is very well reflected in the retrievals. The two most important sources of error are the relative uncertainty in the liquid water path and the unknown effects of multiple scattering. For small values the relative uncertainty in the liquid water path exceeds acceptable values so that the retrieval of droplet concentration becomes impossible. Multiple scattering in calculated extinction profiles will increase the retrieved droplet concentration, but a general guideline on its potential to contaminate the results cannot be given here. For our purposes we have neglected it when performing the retrievals. As it turned out, the droplet concentration was underestimated. A 10% change in the multiple scattering factor cannot nearly account for the difference between the observations and the retrievals on 4 September, but could account for the differences on 19 April.

Improvements to the retrieval technique are possible in four ways. First, the reliability of liquid water path estimates could be improved if the sensitivity of liquid water detection is increased at low liquid water path, for example, by including an extra 94-GHz microwave channel. Further work on improving the precision of liquid water retrieval techniques would similarly aid in reducing the errors of the droplet concentration retrieval technique.

Second, the technique can be improved if better estimates of cloud thickness are available. This can primarily be done by better cloud-top detection using a radar with higher transmitting power, or decreasing the radar wavelength. The radar used to derive cloud top is not the most ideal system suited for such observations as temperature and humidity fluctuations contribute to the signal returns. Radars with a higher operation frequency are more tuned to the detection of cloud droplets and, thus, would be capable of improved precision in cloud-top detection. For the case of 19 April it was shown that for a limited time period the algorithm to detect cloud top did not perform well. This appeared to be due to the presence of another layer of high reflectivity in the proximity of cloud top.

Third, the technique can be improved if a more powerful lidar would enable the retrieval of the extinction profile at a higher resolution. The more points that are available on the lidar extinction curve, the easier it is to apply the curve-fitting technique necessary to adjust the observed extinction curve to the theoretical extinction curve.

Fourth, if the amount of liquid water in a drizzle mode could be measured remotely, for example by using radars with different wavelengths or by using a Doppler capability, this would facilitate retrievals of droplet concentration under drizzling conditions.

Acknowledgments. This work was accomplished while the first author was on leave at the International Research Center for Telecommunication–Transmission and Radar (IRCTR) at Delft University of Technology and at KNMI, De Bilt, Netherlands. The hospitality of staff at IRCTR and KNMI was much appreciated. Gerard Kos of ECN made available the in situ aircraft data. We thank Stuart Young and David de Wolf for discussions on multiple scattering issues during the course of this study.

APPENDIX

Analysis of Uncertainty in the Droplet Concentration Retrieval Technique

The uncertainty in the droplet concentration retrieval can be computed by first addressing the uncertainty δD in the parameter D and then determining how this uncertainty propagates into the retrieval of the droplet concentration. Using Eq. (4), the relative uncertainty in D is defined as

$$\frac{\delta D}{1 - D} = 2\frac{\delta h}{h} - \frac{\delta \mathrm{LWP}}{\mathrm{LWP}}, \tag{A1}$$

where the two terms on the right side of the equation represent the relative uncertainty in h and in LWP. To determine the uncertainty in the retrieval of the droplet concentration it is important to distinguish between the uncertainty in the extinction profile as modeled by Eq. (1) ($\delta\sigma_M$), and the uncertainty in the extinction profile as retrieved from the lidar signal profiles ($\delta\sigma_T$). The model of extinction is a function of the parameters D and N, where D is a function of h and of LWP.

Using Eqs. (1) and (4) it follows that

$$\delta\sigma_M(z) = \frac{1}{3}\sigma_M(z)\left(-4\frac{\delta h}{h} + 2\frac{\delta \mathrm{LWP}}{\mathrm{LWP}} + \frac{\delta N}{N} - 2\frac{\delta z_B}{z - z_B}\right), \tag{A2}$$

where we neglect for the moment any errors caused by variability in the factor $A(\alpha)$. The terms on the right-hand side of (A1) and (A2) could have been written in

terms of absolute values. However, in the current form they allow for inspection of the occurrence of possible compensating errors. The uncertainty δh is a function of δz_B but the latter is much smaller than corresponding uncertainties in the determination of cloud top, so δh is principally a function of uncertainties in cloud-top measurements. We set it to 15 m, although this may vary depending on the strength of the signal returns.

The uncertainty in the determination of LWP is uncertain because of ambiguities of the liquid water path estimation from the downwelling radiation. Different retrieval techniques are employed, each of which incurs different uncertainties. Erkelens et al. (1998a,b) demonstrate that the linear retrieval techniques can yield LWP offsets because of the difficulty in assigning a climatological value for the retrieval constants and ambiguities in the modeling of liquid water content. The new technique of Erkelens et al. (1998a,b), which employs radar cloud height in the estimation of liquid water path, is much less prone to the occurrence of offsets. The assignment of an uncertainty in LWP implies that for small LWP the relative uncertainty in Eq. (A2) can increase to very high levels. Based on the noise levels of the radiometer, plus an averaging time of 10 min, the uncertainty in LWP is minimally 10 g m^{-2}. Calibration drifts of such radiometers would appear in the records as drifts in the brightness temperature offsets during clear (i.e., noncloudy) conditions. No such drifts were observed, so the calibration was stable.

The uncertainty in determining z_B can be observed from Fig. 3. Here a fitted profile was compared with a modeled profile of extinction, where the value of z_B was optimized between two digitization levels (30 m apart) using the procedure outlined in section 3c. For most clouds observed during the experiments the extinction reaches a level exceeding 2 km^{-1} within 5 m above cloud base. We believe that the fitting procedure improves the accuracy of the cloud-base estimate to 1–2 m.

The uncertainty in the retrieved extinction curve is mostly due to the uncertainty in assigning an appropriate multiple scattering factor η to the solution of the Ricatti equation. We make the assumption that it is constant with range, so that the inverted extinction profile has the functional form

$$\sigma_T(z) = \frac{\exp(S - S_m)}{\left[\sigma_m^{-1} + 2\eta \int_z^{z_m} \exp(S - S_m)\, dz'\right]}, \quad \text{(A3)}$$

where σ_T is the value of the extinction at the height z_m from which the inversion is started, S is the natural logarithm of the range-squared corrected lidar signal, and S_m is the natural logarithm for the range-squared corrected lidar signal at height z_m (Klett 1983). The assumption of a constant η is almost certainly incorrect, but it provides for a simple means of assessing its influence on the retrieval. The value of η is allowed to vary between 1.0 (no multiple scatter) and 0.90. We find, not surprisingly, that the uncertainty in retrieved extinction increases with altitude in the cloud. However, on average, the extinction at 150 m above cloud base for $\eta = 0.9$ is different from the extinction for $\eta = 1.0$ by no more than 10%. For each 10-min estimate of the extinction profile the uncertainty in the extinction profile $\delta\sigma_T(z)$ can thus be estimated.

The final uncertainty estimated by fitting the theoretical extinction to the observations is estimated at

$$[\delta\sigma(z)]^2 = [\delta\sigma_T(z)]^2 + [\delta\sigma_M(z)]^2. \quad \text{(A4)}$$

The fit minimizes the sum of the squares so that

$$M = \sum_i [\delta\sigma(z)]^2, \quad \text{(A5)}$$

where the summation is over i points on the extinction curve. Combining (A2), (A4), and (A5) a quadratic equation in $\delta N/N$ is formed, which can be solved for each extinction profile. The uncertainty determined in this manner varies primarily as a result of the variations in the relative uncertainty δLWP/LWP and as a result of a failure of the retrieved σ profiles to match the model represented by Eq. (1). The latter case does not mean that concentration retrievals are impossible using this technique but rather that our model is inadequate.

REFERENCES

Albrecht, B. A., C. W. Fairall, D. W. Thomson, A. B. White, and J. B. Snider, 1990: Surface-based remote sensing of the observed and the adiabatic liquid water content of stratocumulus clouds. *Geophys. Res. Lett.,* **17,** 89–92.

Apituley, A., A. van Lammeren, and R. Sok, 1998: Cloud properties derived by the RIVM high temporal resolution lidar and the Vaisala CT75K lidar ceilometer. *Proc. 19th Int. Laser Radar Conf.,* Vol. 1, Annapolis, MD, Optical Society of America, 139–142.

Babb, D. M., J. Verlinde, and B. A. Albrecht, 1999: Retrieval of cloud microphysical parameters from 94-GHz radar Doppler power spectra. *J. Atmos. Oceanic Technol.,* **16,** 489–503.

Betts, A. K., 1983: Thermodynamics of mixed stratocumulus: Saturation point budgets. *J. Atmos. Sci.,* **40,** 2655–2670.

Boers, R., 1997: Simultaneous retrievals of cloud optical depth and droplet concentration from solar irradiance and microwave liquid water path. *J. Geophys. Res,* **102,** 29 881–29 891.

——, and R. M. Mitchell, 1994: Absorption feedback in stratocumulus clouds: Influence on cloud top albedo. *Tellus,* **46A,** 229–241.

de Wolf, D. A., H. W. J. Russchenberg, and L. P. Ligthart, 1999: Estimates of incoherent-scattering contribution to lidar backscatter from clouds. *Appl. Opt.,* in press.

Dong, X., T. P. Ackermann, E. E. Clotiaux, P. Pilewskie, and Y. Han, 1997: Microphysical and radiative properties of boundary layer stratiform clouds deduced from ground-based measurements. *J. Geophys. Res.,* **102,** 23 829–23 843.

——, ——, and ——, 1998: Parameterisations of the microphysical and radiative properties of boundary layer stratus from ground-based measurements. *J. Geophys. Res.,* **103,** 31 681–31 693.

Erkelens, J. S., H. W. J. Russchenberg, S. C. H. M. Jongen, and M. H. A. J. Herben, 1998a: Cloud liquid water profile estimation combining radar and radiometer. *Proc. Eighth URSI Commission F Triennial Open Symp., Wave Propagation and Remote Sensing,* Aveiro, Portugal, Telecom Portugal, 167–170.

——, ——, ——, and ——, 1998b: Combining radar and microwave radiometer for cloud liquid water retrieval. *Proc. 28th European*

Microwave Conf. Vol. 2, Amsterdam, Netherlands, IEEE/MTT, 67–72.

Fernald, F. G., 1984: Analysis of atmospheric lidar observations: Some comments. *Appl. Opt.,* **23,** 652.

Frisch, A. S., C. W. Fairall, and J. B. Snider, 1995: Measurement of stratus cloud and drizzle parameters with a K_a-band Doppler radar and a microwave radiometer. *J. Atmos. Sci.,* **52,** 2788–2799.

Fox, N. I., and A. J. Illingworth, 1997: The retrieval of stratocumulus cloud properties by ground-based cloud radar. *J. Appl. Meteor.*, **36,** 485–492.

Gossard, E. E., and R. G. Strauch, 1983: *Radar Observation of Clear Air and Clouds.* Elsevier, 280 pp.

——, J. B. Snider, E. E. Clothiaux, B. Martner, J. S. Gibson, R. A. Kropfli, and A. S. Frisch, 1997: The potential of 8-mm radars for remotely sensing cloud drop size distributions. *J. Atmos. Oceanic Technol.,* **14,** 76–87.

Han, Q., W. B. Rossow, and A. A. Lacis, 1994: Near-global survey of effective droplet radii in liquid water clouds using ISCCP data. *J. Climate,* **7,** 465–497.

Klett, J. D., 1983: Stable analytical inversion solution for processing lidar returns. *Appl. Opt.,* **20,** 211–220.

Knight, C. A., and L. J. Miller, 1993: First radar echoes from cumulus clouds. *Bull. Amer. Meteor. Soc.,* **74,** 179–188.

——, and ——, 1998: Early radar echoes from small, warm cumulus: Bragg and hydrometeor scattering. *J. Atmos. Sci.,* **55,** 2974–2992.

Leontyeva, E., and K. Stamnes, 1994: Estimation of cloud optical thickness from ground-based measurements of incoming radiation in the Arctic. *J. Climate,* **7,** 566–578.

——, ——, and J. A. Olseth, 1994: Cloud optical properties at Bergen (Norway) based on the analysis of long-term solar irradiance records. *Theor. Appl. Climatol.,* **50,** 73–82.

Paluch, I. R., C. A. Knight, and L. J. Miller, 1996: Cloud liquid water and radar reflectivity of nonprecipitating cumulus clouds. *J. Atmos. Sci.,* **53,** 1587–1603.

Papatsoris, A. D., 1994: Implication of super-large drops in millimetre-wave radar observations of water clouds. *Elec. Lett.,* **30,** 1799–1800.

Peter, R., and N. Kämpfer, 1992: Radiometric determination of water vapor and liquid water and its validation with other techniques. *J. Geophys. Res.,* **97,** 18 173–18 183.

Politovich, M. K., B. Boba Stankov, and B. E. Martner, 1995: Determination of liquid water content using combined remote sensors. *J. Appl. Meteor.,* **34,** 2060–2075.

Russchenberg, H., 1992: Ground-based remote sensing of precipitation using a multi-polarized FM-CW Doppler radar. Ph.D. thesis, Delft University of Technology, 206 pp.

——, V. K. C. Venema, A. C. A. P. van Lammeren, and A. Apituley, 1998: Cloud measurements with lidar and a 3 GHz radar. Final Report for ESA, Contract PO 151912, 25 pp.

Sassen, K., and L. Liao, 1996: Estimation of cloud content by W-band radar. *J. Appl. Meteor.,* **35,** 932–938.

Spinhirne, J. D., R. Boers, and W. D. Hart, 1989: Cloud-top liquid water from lidar observations of marine stratocumulus. *J. Appl. Meteor.,* **28,** 81–90.

Stephens, G. L., 1978: Radiation profiles in extended water clouds. *J. Atmos. Sci.,* **35,** 2111–2122.

Twomey, S. A., M. Piepgras, and T. L. Wolfe, 1984: An assessment of the impact of pollution on global cloud albedo. *Tellus,* **36B,** 356–366.

Young, S. A., 1995: Analysis of lidar backscatter profiles in optically thin clouds. *Appl. Opt.,* **34,** 7019–7031.

Westwater, E. R., and F. O. Guiraud, 1980: Ground-based microwave radiometric retrieval of precipitable water vapor in the presence of cloud with high liquid content. *Radio Sci.,* **15,** 947–957.